Dalton Transactions

ROYAL SOCIETY OF CHEMISTRY

PAPER

View Article Online
View Journal | View Issue

Cite this: *Dalton Trans.*, 2023, **52**, 13517

G-quadruplex DNA selective targeting for anticancer therapy: a computational study of a novel Pt^{II} monofunctional complex activated by adaptive binding†

Daniele Belletto,[a] Fortuna Ponte,[a] Nico Sanna,[b] Stefano Scoditti *[a] and Emilia Sicilia [a]

Targeting of G-quadruplex (G-Q) nucleic acids, which are helical four-stranded structures formed from guanine-rich nucleic acid sequences, has emerged in recent years as an appealing opportunity for drug intervention in anticancer therapy. Small-molecule drugs can stabilize quadruplex structures, promoting selective downregulation of gene expression and telomerase inhibition and also activating DNA damage responses. Thus, rational design of small molecular ligands able to selectively interact with and stabilize G-Q structures is a promising strategy for developing potent anti-cancer drugs with selective toxicity towards cancer cells over normal ones. Here, the outcomes of a thorough computational investigation of a recently synthesized monofunctional Pt^{II} complex (**Pt1**), whose selectivity for G-Q is activated by what is called adaptive binding, are reported. Quantum mechanics and molecular dynamics calculations have been employed for studying the classical key steps of the mechanism of action of Pt^{II} complexes, the conversion of the non-charged and non-planar **Pt1** complex into a planar and charged Pt^{II} (**Pt2**) complex able to play the role of a G-Q binder and, finally, the interaction of **Pt2** with G-Q. The information obtained from such an investigation allows us to rationalize the behavior of the novel Pt^{II} complex proposed to be activated by adaptive binding toward selective interaction with G-Q or similar molecules and can be exploited for designing ligands with more effective recognition ability toward G-quadruplex DNA.

Received 17th August 2023,
Accepted 1st September 2023

DOI: 10.1039/d3dt02678g

rsc.li/dalton

Introduction

Although genomic DNA is commonly arranged in the canonical right-handed B-type double helix discovered by Watson–Crick in 1953, many alternative structural conformations can exist since DNA and RNA can arrange in non-B secondary structures in living cells, such as four-stranded DNA structures called G-quadruplexes (G-Qs).[1,2] The building blocks of G-quadruplexes are G-quartets that are held together by Hoogsteen hydrogen bonding between four guanines. Planar G-quartets stack on top of each other, forming four-stranded helical structures. The stabilization of these structures is strongly dependent on the established π–π stacking interactions and electrostatic interactions between guanine carbonyl groups and monovalent (Na^+, K^+) or bivalent cations (Mg^{2+}, Ca^{2+}).[3] According to the results of numerous structural analyses, G-quadruplex DNA structures are highly polymorphic and can be categorized into various families. For example, they are classified as parallel or antiparallel, depending on the orientation of the strands, or can be inter- or intra-molecularly folded. Many detailed reviews are available for perusal in the literature[4,5] dealing with these categorizations. All kinds of G-Q arrangements in various biological contexts can be further stabilized by the binding of small molecules;[6,7] whose role is to inhibit the unwinding of G4 to other nucleic acid species. This small-molecule intermediation and stabilization task is the basis of a wide range of G-Q-mediated biological effects, most of which have been studied for their possible exploitation in therapeutic approaches, mainly for fighting human cancer.[8] G-quadruplex DNA structures predominantly exist in the chromosomal telomeric sequences and the promoter regions of numerous oncogenes. The formation of G-Q structures within the telomeric DNA causes the inhibition of telomerase activity, thereby interfering with telomere maintenance in cancer

[a]*Department of Chemistry and Chemical Technologies, Università della Calabria, 87036 Arcavacata di Rende, CS, Italy. E-mail: stefano.scoditti@unical.it*
[b]*Department for Innovation in Biology Agro-Food and Forest Systems (DIBAF), University of Tuscia, Largo dell'Università snc, 01100 Viterbo, Italy*

†Electronic supplementary information (ESI) available: Parallel-stranded G-quadruplex structure, fully optimized geometries of stationary points, additional free energy profiles, outcomes of MD simulation analysis, contributions to the MM-GBSA binding free energy, and developed MD parameters for **Pt2**. See DOI: https://doi.org/10.1039/d3dt02678g

cells,[9] while G-Q DNA formed in promoter regions modulates gene transcription.[10] Thus, rational design of small molecule ligands for selectively interacting and stabilizing either or both the telomeric G-Q and promoter G-Q of oncogenes has been identified as a promising strategy for the development of anticancer drugs with selective toxicity towards cancer cells over healthy ones.[11]

Even though most reported quadruplex DNA binders are purely organic compounds, many metal complexes acting as small molecule G-Q-ligands have attracted a lot of interest, as they are able to interact strongly and selectively with quadruplex nucleic acids, thanks to their characteristic structural features, various charges, and additional advantageous properties.[12,13] As a very important class of planar metal complexes, Pt^{II} coordination complexes have been intensively studied as possible GQ binders and/or stabilizers. Pt^{II} complexes can achieve a relatively high binding affinity to G-Qs that can be properly tuned by varying the ligands.[14–18] Nevertheless, the square-shaped coordination to the Pt^{II} cation that provides the necessary planar geometry for good π–π stacking with G-quartets is the cause of poor selectivity over duplex DNA.[19] Recently, the synthesis and characterization of a new Pt^{II} complex able to manifest its selective binding activity only after activation have been reported.[20] The structure of the complex, which from now on will be named **Pt1** as in the reference paper, is shown in Scheme 1. The calculated and experimental values of the most relevant geometrical parameters are compared in the same scheme. The very good agreement between theory and experiments proves the appropriateness of the adopted computational protocol. The ligands in the coordination sphere of the Pt center are a bidentate cyclometalated ligand, a monodentate N-heterocyclic carbene ligand and a chloride anion.

The donor nitrogen atom of the pyridine substituent on carbene is not coordinated to the metal center. However, chlorido ligand dissociation allows the coordination of the pyridine nitrogen, and the **Pt1** complex, which is neutral and non-planar with a freely rotating N-heterocyclic carbene ligand, transforms into a charged and planar complex, named **Pt2** (see Scheme 1).

The newly formed **Pt2** complex possesses the appropriate characteristics to bind and stabilize G-Q DNA. More importantly, the authors suggest that Cl^- ligand release, new Pt–N bond formation and, eventually, hydrolysis are assisted by G-Q binding. The strategy used to increase the selectivity is based on what the authors define as "adaptive binding kinetics", which is different with respect to all the previously proposed G-Q targeted drugs. This mode of adaptive G-Q binding activation can represent a complementary strategy that can be exploited for designing compounds selectively targeting G-Q DNA. This is the reason why we have considered it relevant to obtain more detailed information at the atomistic level on the mechanism by which the **Pt1** complex is converted into the **Pt2** one once it enters the cell, and the mode of interaction and binding of the formed Pt^{II} complex with G-Q DNA. To this aim, in order to rationalize the experimental findings, in the present paper, both quantum-mechanical DFT computations and all-atom classical Molecular Dynamics (MD) calculations have been carried out starting from the information concerning the mechanism of action of classical Pt^{II} drugs.

Computational details

The Gaussian 16 package has been used to perform density functional theory quantum mechanical calculations.[21] For a better reproduction of the experimental values of the geometrical parameters of the **Pt1** complex, calculations have been carried out using different functionals and basis sets. As a result of this preliminary test, the hybrid Becke three parameter exchange functional combined with the Lee–Yang–Parr correlation functional, B3LYP,[22,23] has been chosen to carry out calculations together with the relativistic compact Stuttgart/Dresden (SDD) effective core potential[24] and the associated split valence basis set. The standard 6-31G** basis set of Pople has been employed to describe the rest of the atoms in the system. The role that should be played by the interaction of the initial **Pt1** complex with G-Q in the process leading to the generation of **Pt2** has been further examined by performing quantum mechanical DFT computations. The displacement of both chlorido and water ligands by the pyridine nitrogen and the substitution of chloride by water have been studied quantum-mechanically using a tractable G-Q model. The G-quadruplex structure formed in a human VEGF promo-

	X-Ray	Theoretical
Distance (Å)		
Pt-N1	2.0683	2.113
Pt-Cl2	2.4027	2.453
Pt-C3	1.9757	2.006
Pt-C4	1.9636	1.981
Angle (°)		
N1-Pt-C4	172.49	175.6
Cl2-Pt-N1	95.27	95.6
Cl2-Pt-C3	176.1	174.6
Cl2-Pt-C	90.33	89.5
Dihedral Angle (°)		
Pt-C4-N5-C6	0.81	0.7
C4-N7-C8-N9	40.97	50.4

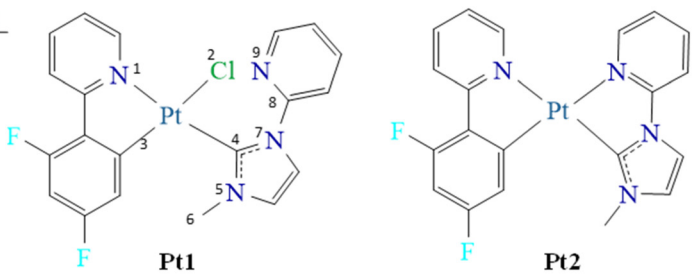

Scheme 1 Schematic representation of the geometrical structure of the investigated **Pt1** and **Pt2** complexes along with the calculated values of the most relevant geometrical parameters for the **Pt1** complex compared with the experimental counterparts.

ter, a monomeric parallel-stranded quadruplex (PDB ID 2M27),[25] has been used according to experiments.[20] The adopted G-Q structure is reported in Fig. S1 of the ESI.† A planar G-tetrad, as shown in Fig. S2,† displaying *C*4 symmetry stabilized by a centrally located potassium cation situated below the tetrad plane, has been cut from the G-quadruplex structure used for carrying out MD simulations. The coordinates of the hydrogen atoms bound to the nitrogen atoms at the N9 position of each guanine have been frozen in order to avoid the unrealistic distortion of the G-Q portion included in the QM calculations because of the absence of the other structures used for MD simulations. The optimization of the stationary points has been performed while maintaining the B3LYP-D3 functional with the basis sets used for the other calculations of the **Pt1** complex, while all the atoms of the quadruplex DNA portion have been treated with the standard 3-21G (d) basis set for reducing the computational effort and carrying out the required maximum number of attempts to locate the transition states. Aiming at clarifying how the interactions with the quadruplex DNA can influence the course of the examined reactions, non-covalent interactions (NCIs) have been investigated by using the RDG (reduced density gradient) analysis proposed by Johnson *et al.*,[26] implemented in the Multiwfn 3.8 software.[27] Nonbonding interactions have been taken into consideration including the atom pair-wise additive scheme for the Grimme dispersion corrections,[28] the DFT-D3 method. Frequency calculations have been performed at the same level of theory for all located stationary points to confirm the nature of their minima and transition states and for zero-point energy correction calculations. The intrinsic reaction coordinate (IRC) analysis has been used to check the appropriate connection of intercepted transition states with the corresponding minima. The influence of solvation on reactivity has been taken into consideration when performing geometry optimizations in an implicit solvent using Tomasi's implicit polarizable continuum model (PCM),[29–31] water as the solvent to simulate the physiological environment (ε = 78.4) and the UFF set of radii to build up the cavity. In order to simulate the interaction with canonical DNA, guanine has been used as a model of an interaction site of DNA, while methionine has been employed to simulate the interaction with biological molecules rich in sulphur. Enthalpies and Gibbs free energies have been calculated to be 298 K and 1 atm from total energies including zero-point and thermal corrections on the basis of standard statistical procedures.[32] Relative Gibbs free energies (ΔG) have been calculated for all the stationary points located along the reaction pathways with respect to the free energy of the species fixed as the zero reference energy of the system. In order to study, by means of molecular dynamics simulations, the interaction of the **Pt2** complex with G-Q, the G-quadruplex structure described above has been used. The starting geometry of G-Q/**Pt2** has been taken from the structure obtained experimentally.[20] The platinum metal centre has been parametrized by using both Gaussian 16 and MCPB.py[33] in the Amber 16 package[34] and the details can be found in the ESI.† For the metal centre created model, geometry optimization and frequency calculations have been carried out using the SDD effective core potential and the corresponding split valence basis set to describe the Pt atom and the 6-311G** basis set for the rest of the atoms employing Gaussian 16. Gaussian 16 has also been employed to calculate the Merz–Kollman ESP charges for the metal centre model, while MCPB.py has been used to perform RESP charge fitting. Topology and coordinate files have been generated by means of the command-line program tleap of Amber 16 using the standard DNA.bsc1[35] and gaff force fields[36,37] together with the newly generated parameters for the metal centre. An octahedral box of water molecules around the G-Q/**Pt2** adduct with a 14 Å buffer distance has been built up using a TIP3P solvation model.[38] Sodium ions have been added to neutralize the system. The system has been relaxed prior to the molecular dynamics simulations using 1000 minimization steps with a cutoff distance of 15.0 Å and constant volume periodic boundaries. G-Q and **Pt2** have been held fixed during this initial minimization by using a force constant of 500 kcal mol^{-1}. This has been followed by 2500 minimization steps for the whole system including the DNA with the same cutoff distance and constant volume periodic boundaries. The system has then been heated from 0 K to 300 K over 10 000 steps for a total of 20 ps. The SHAKE algorithm has been implemented to constrain bonds involving hydrogen. During the heating, the DNA and **Pt2** have been weakly restrained by a force constant of 10 kcal mol^{-1} while keeping constant volume periodic boundaries and the same cutoff distance. Equilibration followed by molecular dynamics simulations for 300 ns at 300 K was performed under similar conditions with a 2 fs interval with no restraints on DNA. The SHAKE algorithm was used to constrain bonds involving hydrogen and a cutoff distance of 15.0 Å was maintained. A constant pressure periodic boundary with an average pressure of 1 atm and isotropic position scaling with a relaxation time of 2 ps were used. The CPPTRAJ script[39] and VMD software[40] were used to process and analyse molecular dynamics simulations.

Results and discussion

The outcomes of our quantum mechanical and MD exploration aiming at shedding light on the mechanism of action of the novel synthesized complex **Pt1**, proposed as a platinum compound that can bind to G-Q DNA selectively, will be illustrated in the next paragraphs. It is worth mentioning that the **Pt1** complex, before chlorido ligand release and coordination of the N atom of the pyridine substituent on the carbene ligand to the Pt atom, is a monofunctional complex. Monofunctional platinum drugs, proposed as non-classical alternatives to Pt^{II} complexes, in analogy to cisplatin and its derivatives, are subject to aquation, which is prevented in blood due to the relatively high concentration of chlorido ions and is promoted inside the cell where the chloride concentration decreases significantly. Aquation and the following DNA platination are known to be the two key activation steps

of platinum-based drugs when they enter the cell. Unlike cisplatin, however, monofunctional complexes are able to form only a single bond with DNA as they contain only one labile ligand and, as it happens for the most successful monofunctional Pt^{II} complex phenanthriplatin, additional factors should assist the observed cytotoxic action. The presence of the extended aromatic system of the phenanthridine ligand, in the case of the phenanthriplatin complex, plays a key role in determining the cytotoxic profile of the complex.[41,42] For the monofunctional **Pt1** complex, the experiments have demonstrated a marked preference to bind to G-Q over double-stranded DNA (dsDNA). Therefore, in the case under examination, the structural rearrangement for converting **Pt1** into **Pt2** plays a key role in determining the activity profile of the complex. The interaction with G-Q should favour the geometrical rearrangement of the monofunctional **Pt1** complex, leading to the formation of **Pt2** that is the real active species able to bind and stabilize G-Q DNA. Starting from these premises, the whole range of different reactions the **Pt1** complex should undergo when it enters the cell has been examined.

Quantum mechanical simulation of Pt1 aquation, guanine binding and methionine interaction

The commonly tested steps of aquation, binding to guanine, as a model of a purine base site of DNA, and interaction with methionine, as a model of sulfur-containing compounds that can decrease platination levels thanks to their high binding affinity for Pt, have been investigated here for complex **Pt1** using quantum mechanical DFT calculations. The calculated free energy profiles in water are reported in Fig. 1 along with the optimized structures of the located stationary points.

The aquation reaction takes place by a typical second-order nucleophilic substitution (S_N2) of the chlorido anion with a water molecule as shown in Fig. 1a. The pseudo-trigonal bipyramidal structure of the transition state for the associative displacement of the chlorido ligand lies 15.9 kcal mol^{-1} above the zero reference energy of the first formed adduct. Formation of the aquated product, which from now on will be named $\mathbf{Pt1_{wat}}$, is endergonic by 4.4 kcal mol^{-1}. The comparison of the range of higher values[43,44] previously calculated with those experimentally estimated for the cisplatin aquation barrier further confirms that the carbon atom at the *trans* position to the chlorido leaving ligand is efficacious in favouring the dissociation[45,46] and activation by aquation to occur very quickly.

After the aquation step, the mechanism of action of classical Pt^{II} complexes involves DNA binding by coordination of the Pt atom to, principally, the N7 position of guanine bases. Therefore, the interaction of the aquated form of the **Pt1** complex with a guanine molecule, as a DNA model, has been explored and the calculated free energy profile is shown in Fig. 1b.

The transition state assuming once again a pseudo-trigonal bipyramidal geometry corresponding to the very favorable nucleophilic attack occurs, in analogy with many other examined situations, along a S_N2 mechanism pathway. The calculated barrier is 10.7 kcal mol^{-1} and the displacement reaction is exergonic by 4.7 kcal mol^{-1}.

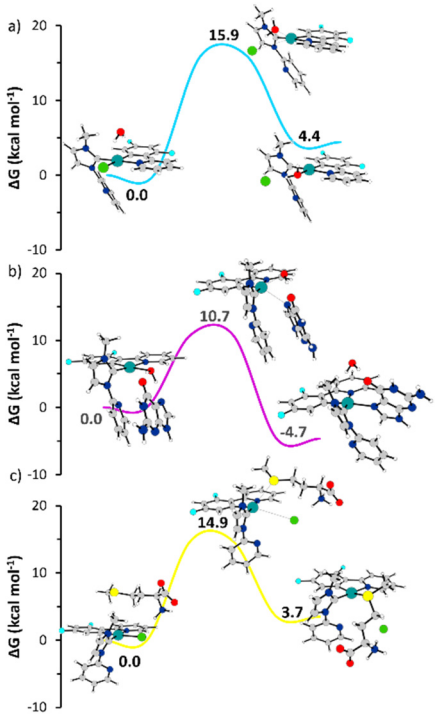

Fig. 1 Calculated free energy profiles in water describing (a) the aquation reaction of **Pt1**, (b) guanine attack of the aquated form of **Pt1** and (c) chloride displacement by methionine. Geometrical structures of the stationary points intercepted along the paths are also reported. Relative energies are in kcal mol^{-1} and calculated with respect the zero reference energy of the initial adduct.

It is well known that the efficacy of Pt complexes might be decreased by the interaction with low-molecular-weight sulfur containing molecules, which are very abundant in human cells and have a high binding affinity for platinum. The calculation of the pathway, using methionine as a model compound that can cause the inactivation of the complex by forming a stable adduct and preventing the drug from reaching the final target and binding to it, has been carried out. The corresponding free energy profile, sketched in Fig. 1c, shows that, after the formation of the first adduct, the height of the energy barrier for the S_N2 displacement of the chlorido ligand by methionine is calculated to be 15.8 kcal mol^{-1}. Formation of the product is endergonic by 1.2 kcal mol^{-1}. These values can be compared with those calculated for cisplatin, which are 16.7 and −4.9 kcal mol^{-1} for the barrier and the reaction energy, respectively.[47] From this comparison, it appears that the deactivation of **Pt1** is as viable as that of cisplatin from a kinetic point of view, but less favored from a thermodynamic point of view.

In order to cover, through our investigation, all the possible reactions involving the **Pt1** complex, the interaction of the intact non-aquated complex with guanine was also examined and, on the other hand, the inactivation of the aquated form

of the complex by the interaction with methionine was examined. The corresponding calculated free energy profiles are reported in Fig. S3 of the ESI.† Attack on guanine and displacement of the chlorido ligand need to occur, so that an energy barrier of 15.8 kcal mol^{-1} is overcome for the occurrence of the formation reaction of the substitution product that is almost thermoneutral, *i.e.* endergonic by only 0.5 kcal mol^{-1}. The inactivation of the **Pt1$_{wat}$** complex, due to the interaction with the methionine sulfur containing model molecule, takes place through a transition state that is higher in energy than the first formed adduct by 14.9 kcal mol^{-1}, while the reaction is endergonic by 3.1 kcal mol^{-1}. On the basis of the results reported in this section, it appears that all the steps that are commonly involved in the mechanism of action of Pt^{II} drugs are viable for the **Pt1** complex. The energy barrier along the aquation reaction pathway is very accessible and significantly lower than that involved in cisplatin aquation generally assumed as a reference value. For the aquated form of the complex, **Pt1$_{wat}$**, the calculated pathway describing guanine binding shows that platination could take place very quickly. Deactivation due to the affinity for sulfur containing molecules is equally feasible.

QM investigation of the structural change allowing the conversion of Pt1 into Pt2

As anticipated above, the peculiarity of the **Pt1** complex is the possibility to transform from an electrically neutral and non-planar platinum complex, which does not fulfill the classical G-Q binders' requirements, into a charged and planar complex, thanks to the chloride displacement by the nitrogen atom of the pyridine ligand.

The hypothesis formulated by the authors of the experimental work is that this conversion is assisted by the interaction with the G-Q target. In order to test both this hypothesis and the mechanism by which this conversion should occur, the reaction that allows the transformation of **Pt1** into **Pt2** has been examined, preliminarily, in the absence of G-Q. As the computational results concerning the aquation of **Pt1** show that the classical displacement of the chlorido ligand by water is amenable, the mechanistic aspects of the process leading to **Pt2** formation have been investigated for both the intact and aquated forms of **Pt1**. The outcomes are summarized in Fig. 2, which shows that the reaction takes place through a typical transition state for a S_N2 substitution rearrangement, allowing the coordination of the pyridine nitrogen.

The transition state for the substitution of the chlorido ligand lies higher in energy than the initial adduct by 13.4 kcal mol^{-1}, while the product formation is calculated to be endergonic by 9.5 kcal mol^{-1}. Water displacement by pyridine appears to be more favorable as the height of the barrier associated with the pseudo trigonal bipyramidal transition state is 11.3 kcal mol^{-1}. The formation of the **Pt2** product accompanied by the definitive release of the water ligand is endergonic by 6.2 kcal mol^{-1}. It is worth mentioning that from the analysis of the structure of the **Pt2** complex, it clearly appears that, with respect to the geometrical arrangement proposed on the basis of the experimental findings, it assumes a distorted square planar geometry. As shown in Fig. 2, the two chelating ligands are not coplanar due to their steric hindrance that does not allow the terminal atoms of the ligands to stay close.

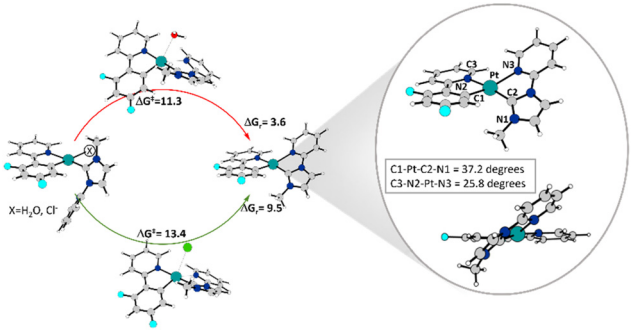

Fig. 2 DFT calculated energy barriers ($\Delta G^{\ddagger}$) and free reaction energies (ΔG_r) in water for the S_N2 substitution rearrangement, allowing the conversion of **Pt1** (green) and its aquated form **Pt1$_{wat}$** (red) into **Pt2**. On the right, the structure of **Pt2** is enlarged to highlight its pseudo-planar geometry. Energies are expressed in kcal mol^{-1}.

How the interaction of **Pt1** with G-Q might influence both the kinetics and the thermodynamics of the process that allows the pyridine nitrogen binding leading to the formation of **Pt2** has been further explored. To this aim, a planar G-tetrad displaying *C*4 symmetry stabilized by a centrally located potassium cation positioned below the tetrad plane has been cut from the G-quadruplex structure (see Fig. S2†) formed in the human VEGF promoter adopted for carrying out MD simulations. An analogous calculation for the displacement of the chlorido ligand in **Pt1** and of water in the corresponding **Pt1$_{wat}$** aquated form by the pyridine substituent of the carbene ligand has been carried out. The results of these computations, for two possible orientations of both **Pt1** and **Pt1$_{wat}$**, are reported in Fig. 3. For the sake of clarity, the portion of G-Q used for the simulation has been reported in wire mode, while the real structure can be found in Fig. S2† of the ESI. Only the structures of the transition states have been reported in Fig. 3, while the optimized geometries of all the stationary points can be found in Fig. S4 and S5.† Both chlorido and water ligands, in the orientation that is named A, are positioned from the side of the G-Q model, whereas in the orientation named B, they are positioned on the opposite side, as better illustrated in the same Fig. S2.† Concerning the orientation A, as shown in Fig. 3a and b, the interaction with G-Q affects the substitution reaction causing an increase in the barrier height, while the stability of the formed products increases. The energy barrier that is needed to overcome becomes, indeed, 21.0 kcal mol^{-1} for chloride and 15.5 kcal mol^{-1} for water with respect to the corresponding calculated barriers in the absence of G-Q that are 13.4 and 11.3 kcal mol^{-1} for chloride and water, respectively. In contrast, the substitution reaction, which is endergonic when the complex does not interact with G-Q, becomes exergonic by 1.1 kcal mol^{-1}

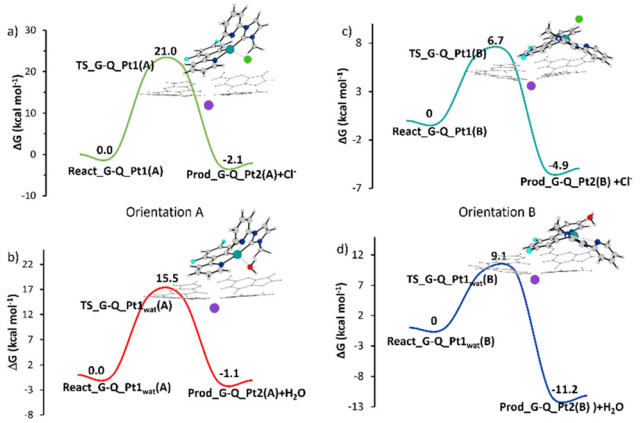

Fig. 3 Calculated free energy profiles in water describing the S_N2 substitution rearrangement in the presence of G-Q allowing the conversion of (a) **Pt1** and (b) its aquated form $\mathbf{Pt1_{wat}}$ into **Pt2** in their orientation named A and that of (c) **Pt1** and (d) its aquated form $\mathbf{Pt1_{wat}}$ into **Pt2** in their orientation named B. Geometrical structures of the intercepted transition states are also reported. Relative energies are in kcal mol^{-1} and calculated with respect the zero reference energy of the initial adduct.

when the water ligand is displaced and by 2.1 kcal mol^{-1} when the chlorido ligand substitution is examined.

Very interesting results are obtained for the second orientation, identified as B, since the interaction with G-Q favors significantly the formation of the **Pt2** complex from both the kinetic and thermodynamic points of view. The energy barriers, calculated for the transition states that allow the release of chlorido and water ligands, are 6.7 and 9.1 kcal mol^{-1}, respectively. The energetics of the reaction leading to the formation of the pseudo-planar **Pt2** complex is −4.9 kcal mol^{-1} when the chloride is displaced and −11.2 kcal mol^{-1} for the water substitution. The interactions that are established with G-Q, very likely, have a stabilizing effect in both cases on the intercepted stationary points. Nevertheless, when the **Pt1** complex, in orientation B, is disposed with the carbene ligand on the side of the G-Q tetrad and directly interacts with it, the driving force represented by the possibility to establish the incoming π–π interactions can explain the generalized stabilization of all the intercepted stationary points. In order to gain deeper insight into the influence of weak interactions on the course of the reactions, the NCI-RDG analysis outcomes for the species located along the reaction pathways have been examined. The graphical plots of NCIs are shown in Fig. 4 for the reaction involving **Pt1** in A and B orientations. The analogous maps for the corresponding aquated $\mathbf{Pt1_{wat}}$ are sketched in Fig. S6 of the ESI.† It appears from these RDG maps that the intermolecular regions are dominated by the green color associated with delocalized weak interactions, while the intensity of the green color is associated with the strength of the interaction. Let us consider, first, the stationary points in orientation A.

Starting from the first adduct formed between the unperturbed **Pt1** complex and quadruplex DNA, it appears that besides the weak π–π stacking interaction established between the phenylpyridine ligand and the two guanines underneath, the most important contribution comes from the interaction classified as a cation–π interaction.[48] This kind of interaction has been classified initially as an electrostatic interaction since a positively charged cation interacts with a negatively charged electron cloud of π systems. Furthermore, it has been suggested that other factors such as induction and dispersion are also important[49] while Yi *et al.* have demonstrated[50] that transition metal cation–π interactions also include covalent characters due to π donations. In the present case, this interaction is established between the Pt center and the pyrimidine

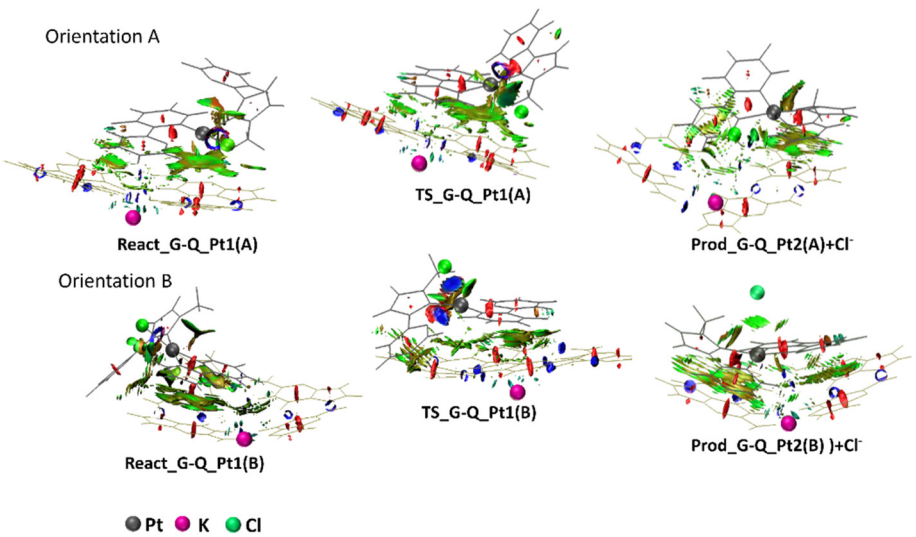

Fig. 4 Plots of the RDG analysis of non-covalent interactions for the stationary points located along the free energy profile, describing the conversion of **Pt1**, in A and B orientations, into **Pt2** in the presence of G-Q.

ring right below it. This interaction that continues to exist in the transition state has to be broken due to the required structural rearrangement that allows the pyridine nitrogen to coordinate with the metal centre. In the resulting product, additional π–π stacking interactions, arising from the pseudo-planarity of the complex, promote its stabilization. When the orientation B is considered, it clearly appears that in the initial adduct, the stabilizing effect is due to the π–π stacking interaction between the phenylpyridine ligand and the guanines underneath. It is evident that a new π–π stacking interaction is going to be established in the transition state structure between the carbene-pyridine ligand and the guanine couple below it. Such an interaction is accomplished in the product due to a lateral displacement of the whole complex as a result of its pseudo planar rearrangement.

An analogous description of the way the intermolecular interactions evolve along the substitution reaction pathways can be given when the water ligand is displaced from the **Pt1$_{wat}$** complex, as it appears from the graphs reported in Fig. S4.†

QM description of the influence of the presence of G-Q on Pt1 aquation

Also, the hypothesis formulated by the authors that the rate of the **Pt1** aquation reaction might be influenced by the interaction with G-Q has been tested. The free energy profiles describing the substitution of the chlorido ligand by water are reported in Fig. 5 together with the structures of the optimized transition states located along these pathways. The optimized structures of all the intercepted stationary points can be found in Fig. S6 and S7 of the ESI.† The same reduced model of G-Q (see Fig. S2†) has been used and the aquation has been examined considering the two orientations of the **Pt1** complex with respect to the G-Q model. The pyridine ring of the carbene ligand is on the opposite side with respect to G-Q in the first orientation named C, while the orientation is named D when the pyridine ring of the carbene ligand is on the same side of the G-Q model.

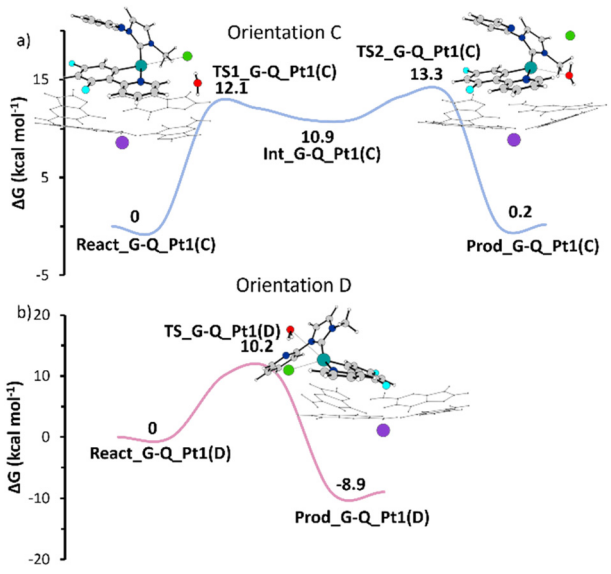

Fig. 5 Free energy profiles in water describing the aquation reaction of **Pt1** in its (a) orientation C and (b) orientation D. Geometrical structures of the intercepted transition states are also reported. Relative energies are in kcal mol^{-1} and calculated with respect to the zero reference energy of the initial adduct.

The way in which the **Pt1** complex interacts with G-Q in the two considered orientations significantly influences the mechanism of the aquation reaction. Indeed, the reaction occurs in a stepwise fashion for the complex in orientation C. The first step consists of the release of the chlorido ligand that occurs after overcoming an energy barrier of 12.1 kcal mol^{-1} calculated with respect to the first adduct formed between G-Q and the entering water molecule assumed as the zero reference energy. A very unstable intermediate is formed, lying 10.2 kcal mol^{-1} above the energy of the entrance channel. The released chloride is substituted by water in the second step where a very low energy barrier of only 2.4 kcal mol^{-1} has to be overcome, leading to the formation of the final aquated product that is almost thermoneutral with respect to the first adduct. In the examined situation, the presence of the quadruplex DNA induces a significant change in the kind of mechanism that from being of the associative type becomes dissociative. The kind of mechanism does not change, instead, with the complex in orientation D and continues to be associative with the water molecule, displacing the chlorido ligand in one step. The height of the barrier for the transition state that allows this transformation to occur is 10.2 kcal mol^{-1} and the reaction is exergonic by 8.9 kcal mol^{-1}. For the rationalization of such behaviours, also in this case, the NCI-RDG analysis outcomes have been used. RDG plots for the species located along the studied pathways are reported in Fig. S8.† From such plots, it appears that when the **Pt1** complex, neutral and non-planar with a freely rotating ligand, adopts the orientation named C, the most important weak interaction that can be established with the quadruplex DNA in the initial adduct is classified as cation–π between the platinum center and the guanine underneath. It is, very likely, such an interaction that allows the chloride to be detached. This interaction is not strong enough to stabilize the first formed intermediate **Int_Pt1_G-Q(C)** that very quickly evolves towards the coordination of the water molecule to the metal center in the second step. Weak π–π interactions between the phenylpyridine ligand and the G-Q guanines slightly stabilize the final aquated product. The whole reaction, indeed, results in being thermoneutral, while **Pt1** aquation is endergonic in the absence of G-Q (Fig. 1). When the complex adopts the D orientation, it can come closer to the G-Q tetrad, establishing strong π–π stacking interactions that stabilize the transition state and the product.

Summarizing the results illustrated in this section, it can be underlined that **Pt1** aquation could occur, as usual for Pt^{II} complexes, as an initial step when the chloride concentration significantly decreases in the cytoplasm inside the cell. The aquation process is facilitated by the *trans* effect and the calculated barrier height is significantly lower than that predicted

for cisplatin and analogous complexes. Aquation can prelude to the decisive step for platinum-based anticancer drugs involved in canonical DNA platination when they enter the nucleus, and this step also results in being easily accessible. Nevertheless, our calculations show that the transformation of **Pt1** into **Pt2**, which allows the **Pt1** complex to become suitable to play the role of the G-Q DNA binder, can take place before the complex comes in close contact with the quadruplex DNA. This mechanistic aspect is worth mentioning as, if **Pt2** is generated before entry into the nucleus, the platination of dsDNA cannot take place and the remaining interaction that can be established is due to intercalation. Furthermore, calculations corroborate the assumption that the interaction of the **Pt1** complex with G-Q facilitates its rearrangement to form the **Pt2** complex, starting from both the intact **Pt1** complex and its aquated form $\mathbf{Pt1_{wat}}$. Weak intermolecular interactions that are established by both **Pt1** and **Pt2** with the adopted G-Q model stabilize both reactants and products, resulting in exergonic reactions. When the complex adopts the orientation named B, the height of the barriers also decreases with respect to the process occurring in the absence of G-Q. Intermolecular interactions between **Pt1** and G-Q also assist the aquation reaction although the final result strongly depends on the mode of the orientation of the complex with respect to the quadruplex.

MD simulation of the interaction of Pt2 with G-Q

Computational outcomes extensively illustrated in the previous sections confirm that the interaction of the **Pt1** complex with G-Q significantly favours its conversion into **Pt2**. Once the coordination of the pyridine nitrogen to the Pt center is realized, a pseudo-planar **Pt2** complex is formed that should be able to bind and stabilize the G-quadruplex. In order to study the binding process and provide insight into the types of interactions established between the G-Q DNA binder and the nucleic acid structure, molecular dynamics simulations have been performed.

On the basis of what has been reported in the reference paper,[20] the monomeric parallel-stranded quadruplex VEGF has been selected as the G-quadruplex system and the reported NMR resolved structure of **Pt2** bound to VEGF has been used for a 300 ns long MD simulation (MD1). Moreover, one additional simulation MD2 has been performed using the same starting geometry. The DNA-binding of the investigated Pt^{II} complex has been investigated and representative structures obtained by RMSD-based clustering from the MD trajectories, showing the interaction of **Pt2** with G-Q, are displayed in Fig. 6.

The all-atom RMSD increases in both MD simulations (Fig. S9† black line), while the RMSD of the guanine atoms (red line) remains stable, suggesting that all the significant variations are caused by the quadruplex flexible loops and flanking bases. The distance between the Pt atom and the O6 carbonyl atoms of the four guanines of the terminal G-tetrad along the trajectories has been plotted in Fig. 7.

In MD1, after an initial settling during the first 100–130 ns, the binding position of **Pt2** becomes stable. In the MD1 simulation, the complex nearly aligns with the potassium ion channel as observed previously for other metal complexes.[51–53] Modeling depicts a different scenario for MD2, as in this case,

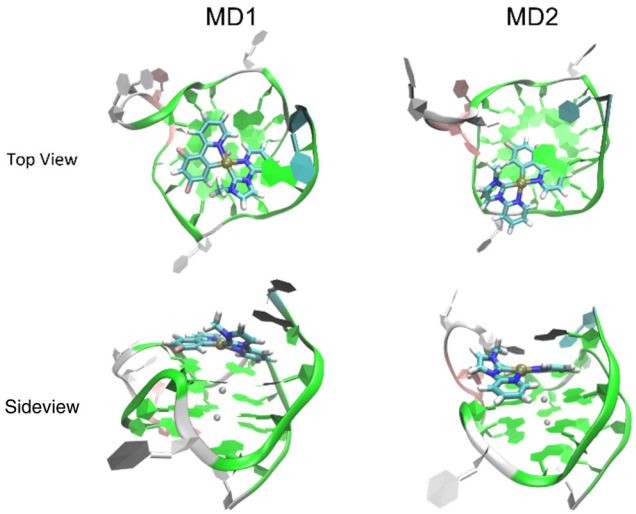

Fig. 6 Top and side views of the binding poses of **Pt2** interacting with G-Q DNA. **Pt2** is shown in the licorice style and guanines are highlighted in green.

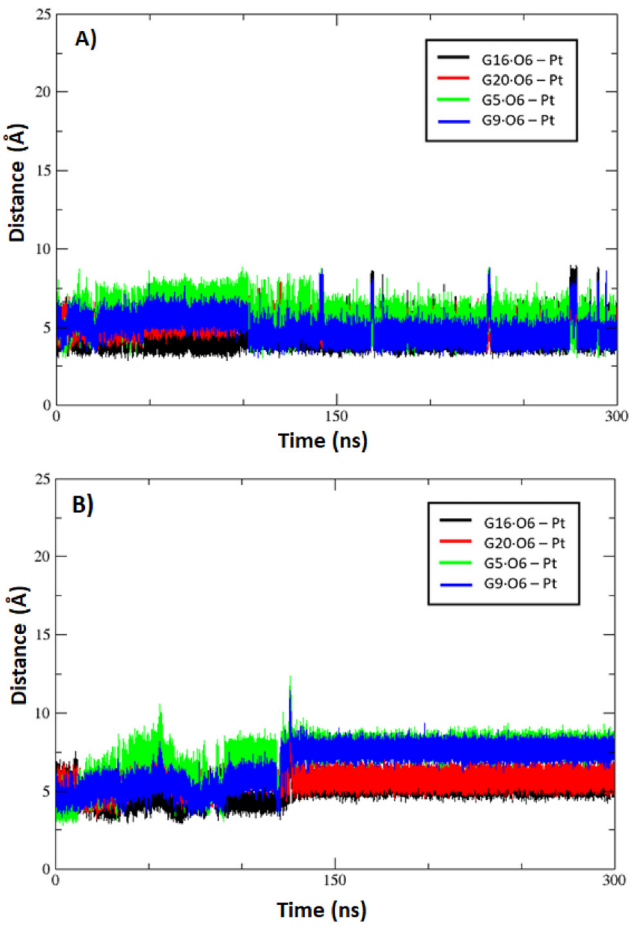

Fig. 7 Distance (Å) between Pt and O6 atoms of the four guanines in the 3′ quartet for (A) MD1 and (B) MD2 simulations.

the binding pose does not tend to align the Pt metal center with the potassium channel, but the complex tends to stay at the edge of the terminal tetrad. In fact, as it is clearly observed in Fig. 7, the platinum–oxygen distances are longer than those in MD1. The "edge" interaction mode shown in MD2 could be due to the pseudo planarity of this complex that decreases the possibility of π–π stacking interaction with the terminal guanine and the electrostatic interaction between the charged Pt center with the π system underneath and the prevailing negatively charged phosphate groups of the backbone. The different ways of interaction of the pseudo-planar complex deduced from QM investigations are confirmed by MD calculations. A better view of the difference between the two binding poses is given by superimposing them as shown in Fig. S10.† The G-Q DNA length calculated as the distance between the two terminal tetrads has been calculated for MD1 and MD2 and in order to get an idea of what the effect of the interaction with **Pt2** is, an extra MD simulation on G-Q alone has been performed. From this analysis, reported in ESI Fig. S11,† no relevant changes, in terms of stretching in the DNA structure, have been found when the complex establishes weak interactions with G-Q.

To evaluate the affinity of **Pt2** for the quadruplex in the two different modes of interaction taken into consideration, binding energies have been extracted using the last 150 ns of simulation by means of the MM-GBSA analysis method present in the MM-PBSA script.[54] The calculated values of −24.8 and −24.6 kcal mol^{-1} have been obtained for MD1 and MD2, respectively. These data suggest that bindings are efficient and, even if binding poses are geometrically different, they have very similar stabilizing effects. The analysis of the different terms that compose the MMGBSA binding energy (see the ESI†) turns out that for MD1, van der Waals interactions are larger than those in MD2, but this gap is filled by a larger electrostatic contribution present in the second simulation MD2.

Molecular dynamics simulations reveal how the complex **Pt2** formed as a consequence of the displacement processes of water or chlorido ligands, investigated *via* quantum mechanical calculations, exhibits two distinct modes of interaction. This double possibility of interaction, reasonably due to the pseudo planarity of the complex, nevertheless leads to stable adducts corroborating the use of this strategy for selective targeting and subsequent stabilization of G-Q DNA. It is worth mentioning that RDG analysis has highlighted how the analogous binding poses of **Pt1** with respect to G-Q influence the kinetics and thermodynamics of substitution reactions.

Conclusions

With the synthesis of a new monofunctional Pt^{II} complex, named **Pt1**, activated by adaptive binding toward the selective interaction with G-quadruplex DNA, a new strategy has been proposed for the design of platinum-based complexes able to act efficiently as G-Q binders. In the present paper, the results of a detailed computational investigation of the whole range of different reactions that the **Pt1** complex should undergo when it enters the cell are illustrated. The key steps of the mechanism of action of Pt^{II} complexes: aquation, guanine binding and methionine interaction, have been examined, demonstrating that all the three reactions are accessible. Due to the positive *trans*-effect, the aquation energy barrier is lower than those for classical Pt^{II} complexes, guanine binding is exothermic and the height of the barrier to overcome is 10.7 kcal mol^{-1}. In addition, deactivation by sulphur rich molecules, simulated using methionine, should occur quickly enough. The most intriguing characteristic of the **Pt1** complex is the possibility to transform from an electrically neutral and non-planar platinum complex, which does not fulfil the classical G-Q binders' requirements, into a charged and planar complex **Pt2**, thanks to the chloride displacement by the nitrogen atom of the pyridine ligand. The reaction has been studied, simulating water's physiological environment, starting from both the intact and aquated complexes. It has been shown that the reaction can take place in both the cases by overcoming accessible barriers, whereas the reaction energies are positive mainly when the chloride has to be replaced. The aquation reaction and the transformation of **Pt1** into **Pt2** have also been examined at the DFT level simulating the presence of G-Q with a downsized model cut from the G-Q structure adopted for carrying out MD simulations. The outcomes demonstrate that the **Pt1** interaction with G-Q significantly affects the investigated reactions and, depending on the particular orientation of the complex, with respect to the G-Q model, very favourable thermodynamics and kinetics can be accomplished. The observed behaviours have been rationalized with the help of the reduced density gradient of non-covalent interactions analysis. Finally, the suitability of the formed pseudo-planar **Pt2** complex to act as a G-Q binder has been corroborated using MD modelling. Computations confirm the affinity of the complex for the quadruplex. It is worth mentioning that the two possible modes of interaction have been extracted from MD simulations: MD1 in which the complex nearly aligns with the potassium ion channel and MD2 in which the complex tends to stay at the edge of the terminal tetrad. The same kind of binding pose has been demonstrated to play a key role in affecting **Pt1** aquation and transformation into **Pt2**.

Conflicts of interest

There are no conflicts to declare.

Acknowledgements

This work has been funded by the Italian Association for Cancer Research, AIRC (ID: 25578) to Dr Fortuna Ponte. S. S. thanks the financial support from ICSC – Centro Nazionale di Ricerca in High Performance Computing, Big Data and Quantum Computing, funded by the European Union –

NextGenerationEU – PNRR, Missione 4 Componente 2 Investimento 1.4. The authors gratefully acknowledge the computing time granted by the CINECA (project IscrC MoAPACT).

References

1 D. Sen and W. Gilbert, *Nature*, 1988, **334**, 364–366.
2 W. I. Sundquist and A. Klug, *Nature*, 1989, **342**, 825–829.
3 E. Largy, J.-L. Mergny and V. Gabelica, *The Alkali Metal Ions: Their Role for Life*, Chapter: Role of Alkali Metal Ions in G-Quadruplex Nucleic Acid Structure and Stability, 2016, pp. 203–258.
4 D. J. Patel, A. T. Phan and V. Kuryavyi, *Nucleic Acids Res.*, 2007, **35**, 7429–7455.
5 S. Burge, G. N. Parkinson, P. Hazel, A. K. Todd and S. Neidle, *Nucleic Acids Res.*, 2006, **34**, 5402–5415.
6 S. Müller and R. Rodriguez, *Expert Rev. Clin. Pharmacol.*, 2014, **7**, 663–679.
7 M. K. Islam, P. J. Jackson, K. M. Rahman and D. E. Thurston, *Future Med. Chem.*, 2016, **8**, 1259–1290.
8 S. Neidle, *Nat. Rev. Chem.*, 2017, **1**, 0041.
9 D. Sun, B. Thompson, B. E. Cathers, M. Salazar, S. M. Kerwin, J. O. Trent, T. C. Jenkins, S. Neidle and L. H. Hurley, *J. Med. Chem.*, 1997, **40**, 2113–2116.
10 A. Siddiqui-Jain, C. L. Grand, D. J. Bearss and L. H. Hurley, *Proc. Natl. Acad. Sci. U. S. A.*, 2002, **99**, 11593–11598.
11 S. Balasubramanian and S. Neidle, *Curr. Opin. Chem. Biol.*, 2009, **13**, 345–353.
12 N. H. Campbell, N. H. A. Karim, G. N. Parkinson, M. Gunaratnam, V. Petrucci, A. K. Todd, R. Vilar and S. Neidle, *J. Med. Chem.*, 2012, **55**, 209–222.
13 S. N. Georgiades, N. H. Abd Karim, K. Suntharalingam and R. Vilar, *Angew. Chem., Int. Ed.*, 2010, **49**, 4020–4034.
14 L. D'Anna, S. Rubino, C. Pipitone, G. Serio, C. Gentile, A. Palumbo Piccionello, F. Giannici, G. Barone and A. Terenzi, *Dalton Trans.*, 2023, **52**, 2966–2975.
15 B. S. McGhie, J. Sakoff, J. Gilbert, C. P. Gordon and J. R. Aldrich-Wright, *Int. J. Mol. Sci.*, 2022, **23**, 10469.
16 D. L. Ang, C. Kelso, J. L. Beck, S. F. Ralph, D. G. Harman and J. R. Aldrich-Wright, *JBIC, J. Biol. Inorg. Chem.*, 2020, **25**, 429–440.
17 I. Ortiz de Luzuriaga, X. Lopez and A. Gil, *Annu. Rev. Biophys.*, 2021, **50**, 209–243.
18 J. Zhang, F. Zhang, H. Li, C. Liu, J. Xia, L. Ma, W. Chu, Z. Zhang, C. Chen, S. Li and S. Wang, *Curr. Med. Chem.*, 2012, **19**, 2957–2975.
19 J. Wang, K. Lu, S. Xuan, Z. Toh, D. Zhang and F. Shao, *Chem. Commun.*, 2013, **49**, 4758.
20 B. Zhu, J. He, W. Liu, X. Xia, L. Liu, B. Liang, H. Yao, B. Liu, L. Ji and Z. Mao, *Angew. Chem.*, 2021, **133**, 15468–15471.
21 M. J. Frisch, G. W. Trucks, H. B. Schlegel, G. E. Scuseria, M. A. Robb, J. R. Cheeseman, G. Scalmani, V. Barone, G. A. Petersson, H. Nakatsuji, X. Li, M. Caricato, a. V. Marenich, J. Bloino, B. G. Janesko, R. Gomperts, B. Mennucci, H. P. Hratchian, J. V. Ortiz, A. F. Izmaylov, J. L. Sonnenberg, D. Williams-Young, F. Ding, F. Lipparini, F. Egidi, J. Goings, B. Peng, A. Petrone, T. Henderson, D. Ranasinghe, V. G. Zakrzewski, J. Gao, N. Rega, G. Zheng, W. Liang, M. Hada, M. Ehara, K. Toyota, R. Fukuda, J. Hasegawa, M. Ishida, T. Nakajima, Y. Honda, O. Kitao, H. Nakai, T. Vreven, K. Throssell, J. A. Montgomery Jr., J. E. Peralta, F. Ogliaro, M. J. Bearpark, J. J. Heyd, E. N. Brothers, K. N. Kudin, V. N. Staroverov, T. A. Keith, R. Kobayashi, J. Normand, K. Raghavachari, A. P. Rendell, J. C. Burant, S. S. Iyengar, J. Tomasi, M. Cossi, J. M. Millam, M. Klene, C. Adamo, R. Cammi, J. W. Ochterski, R. L. Martin, K. Morokuma, O. Farkas, J. B. Foresman and D. J. Fox, *Gaussian 16, Revision C.01*, Gaussian, Inc., Wallin, 2016.
22 A. D. Becke, *J. Chem. Phys.*, 1993, **98**, 5648–5652.
23 C. Lee, W. Yang and R. G. Parr, *Phys. Rev. B: Condens. Matter Mater. Phys.*, 1988, **37**, 785.
24 D. Andrae, U. Häußermann, M. Dolg, H. Stoll and H. Preuß, *Theor. Chim. Acta*, 1990, **77**, 123–141.
25 P. Agrawal, E. Hatzakis, K. Guo, M. Carver and D. Yang, *Nucleic Acids Res.*, 2013, **41**, 10584–10592.
26 E. R. Johnson, S. Keinan, P. Mori-Sánchez, J. Contreras-García, A. J. Cohen and W. Yang, *J. Am. Chem. Soc.*, 2010, **132**, 6498–6506.
27 T. Lu and F. Chen, *J. Comput. Chem.*, 2012, **33**, 580–592.
28 S. Grimme, J. Antony, S. Ehrlich and H. Krieg, *J. Chem. Phys.*, 2010, **132**, 154104.
29 E. Cancès, B. Mennucci and J. Tomasi, *J. Chem. Phys.*, 1997, **107**, 3032–3041.
30 M. Cossi, V. Barone, B. Mennucci and J. Tomasi, *Chem. Phys. Lett.*, 1998, **286**, 253–260.
31 B. Mennucci and J. Tomasi, *J. Chem. Phys.*, 1997, **106**, 5151–5158.
32 H. Cartwright, *Chem. Educ.*, 1999, **4**, 120–121.
33 P. Li and K. M. Merz, *J. Chem. Inf. Model.*, 2016, **56**, 599–604.
34 D. A. Case, R. M. Betz, D. S. Cerutti, T. E. Cheatham III, T. A. Darden, R. E. Duke, T. J. Giese, H. Gohlke, A. W. Goetz, N. Homeyer, S. Izadi, P. Janowski, J. Kaus, A. Kovalenko, T. S. Lee, S. LeGrand, P. Li, C. Lin, T. Luchko, R. Luo, B. Madej, D. Mermelstein, K. M. Merz, G. Monard, H. Nguyen, H. T. Nguyen, I. Omelyan, A. Onufriev, D. R. Roe, A. Roitberg, C. Sagui, C. L. Simmerling, W. M. Botello-Smith, J. Swails, R. C. Walker, J. Wang, R. M. Wolf, X. Wu, L. Xiao and P. A. Kollman, *AMBER 2016*, University of California, San Francisco, 2016.
35 I. Ivani, P. D. Dans, A. Noy, A. Pérez, I. Faustino, A. Hospital, J. Walther, P. Andrio, R. Goñi, A. Balaceanu, G. Portella, F. Battistini, J. L. Gelpí, C. González, M. Vendruscolo, C. A. Laughton, S. A. Harris, D. A. Case and M. Orozco, *Nat. Methods*, 2016, **13**, 55–58.
36 J. Wang, R. M. Wolf, J. W. Caldwell, P. A. Kollman and D. A. Case, *J. Comput. Chem.*, 2004, **25**, 1157–1174.
37 J. Wang, W. Wang, P. A. Kollman and D. A. Case, *J. Mol. Graphics Modell.*, 2006, **25**, 247–260.

38 P. Mark and L. Nilsson, *J. Phys. Chem. A*, 2001, **105**, 9954–9960.
39 D. R. Roe and T. E. Cheatham, *J. Chem. Theory Comput.*, 2013, **9**, 3084–3095.
40 W. Humphrey, A. Dalke and K. Schulten, *J. Mol. Graphics*, 1996, **14**, 33–38.
41 E. Dabbish, N. Russo and E. Sicilia, *Chem. – Eur. J.*, 2020, **26**, 259–268.
42 G. Y. Park, J. J. Wilson, Y. Song and S. J. Lippard, *Proc. Natl. Acad. Sci. U. S. A.*, 2012, **109**, 11987–11992.
43 S. Ahmad, *Polyhedron*, 2017, **138**, 109–124.
44 P. Barretta, F. Ponte, S. Scoditti, V. Vigna, G. Mazzone and E. Sicilia, *J. Phys. Chem. A*, 2022, **126**, 7159–7167.
45 G. Mazzone, S. Scoditti, R. Caligiuri, L. Ricciardi, E. Sicilia, M. G. Lupo, I. Rimoldi, N. Godbert, M. La Deda, A. Ionescu, M. Ghedini, I. Aiello and G. Facchetti, *Inorg. Chem.*, 2022, **61**, 7188–7200.
46 S. Scoditti, E. Dabbish, N. Russo, G. Mazzone and E. Sicilia, *Inorg. Chem.*, 2021, **60**, 10350–10360.
47 S. Scoditti, V. Vigna, E. Dabbish and E. Sicilia, *J. Comput. Chem.*, 2021, **42**, 608–619.
48 D. A. Dougherty, *Science*, 1996, **271**, 163–168.
49 S. Tsuzuki, M. Mikami and S. Yamada, *J. Am. Chem. Soc.*, 2007, **129**, 8656–8662.
50 H.-B. Yi, H. M. Lee and K. S. Kim, *J. Chem. Theory Comput.*, 2009, **5**, 1709–1717.
51 V. Vigna, S. Scoditti, A. Spinello, G. Mazzone and E. Sicilia, *Int. J. Mol. Sci.*, 2022, **23**, 15579.
52 R. Bonsignore, A. Terenzi, A. Spinello, A. Martorana, A. Lauria, A. M. Almerico, B. K. Keppler and G. Barone, *J. Inorg. Biochem.*, 2016, **161**, 115–121.
53 R. Bonsignore, F. Russo, A. Terenzi, A. Spinello, A. Lauria, G. Gennaro, A. M. Almerico, B. K. Keppler and G. Barone, *J. Inorg. Biochem.*, 2018, **178**, 106–114.
54 B. R. Miller, T. D. McGee, J. M. Swails, N. Homeyer, H. Gohlke and A. E. Roitberg, *J. Chem. Theory Comput.*, 2012, **8**, 3314–3321.